

Correlation effects on non-Hermitian point-gap topology in zero dimension: reduction of topological classification

Tsuneya Yoshida¹ and Yasuhiro Hatsugai¹

¹*Department of Physics, University of Tsukuba, Ibaraki 305-8571, Japan*

(Dated: July 20, 2021)

We analyze a zero-dimensional correlated system with special emphasis on the non-Hermitian point-gap topology protected by chiral symmetry. Our analysis elucidates that correlations destroy an exceptional point on a topological transition point which separates two topological phases in the non-interacting case; one of them is characterized by the zero-th Chern number $N_{\text{0Ch}} = 0$, and the other is characterized by $N_{\text{0Ch}} = 2$. This fact implies that correlations allow to continuously connect the two distinct topological phases in the non-interacting case without closing the point-gap, which is analogous to the reduction of topological classifications by correlations in Hermitian systems. Furthermore, we also discover a Mott exceptional point, an exceptional point where only spin degrees of freedom are involved.

I. INTRODUCTION

Topological properties of non-Hermitian Bloch Hamiltonians have been extensively addressed as one of recent hot topics in condensed matter physics¹⁻⁸. For non-Hermitian systems, a variety of novel phenomena have been reported⁹⁻²¹. In particular, the point-gap topology induces topological phenomena which do not have Hermitian counter parts. For instance, the point-gap topology induces exceptional points (EPs) on which both the real and imaginary parts of the energy eigenvalues touch due to the violation of diagonalizability^{1,22-29}. In addition, the point-gap topology induces skin effects which are described by the novel bulk-boundary correspondence^{30,31}; their ubiquity also became clear recently³²⁻³⁸. Platforms of the above non-Hermitian topology extends to a wide range of systems, such as open quantum systems³⁹⁻⁴³, photonic crystals⁴⁴⁻⁵², mechanical metamaterials⁵³⁻⁵⁵, quasi-particles in equilibrium systems⁵⁶⁻⁶², and so on.

Along with the above crucial progress in the non-interacting case, it turned out that correlation effects enrich topological phenomena as is the case of Hermitian systems⁶³⁻⁷³. For instance, it was reported that correlations induce topological ordered states such as fractional quantum Hall states^{63,66} and spin liquid states^{64,65,67}. In addition, a previous work addressed classification of symmetry-protected topological phases with the non-trivial line-gap topology which have Hermitian counter parts⁷⁴. This result implies that the reduction of topological classification of the line-gap topology should be observed as is the case of Hermitian systems. For Hermitian cases, the presence of correlations allow to adiabatically connect topological phases distinguished by a \mathbb{Z} -invariant in the non-interaction case⁷⁵⁻⁷⁸; for instance, a topological phase in eight copies of the Hermitian Kitaev chain can be adiabatically connected with maintaining the relevant symmetry⁷⁵, which indicates the reduction of topological classification $\mathbb{Z} \rightarrow \mathbb{Z}_8$.

Unfortunately, however, correlation effects on the point-gap topology, which is a unique topological struc-

ture for non-Hermitian systems, have not been sufficiently addressed yet^{79,80}. In particular, one may ask whether correlation effects induce the reduction of topological classification of the point-gap topology. In addition, one may also ask whether interactions result in any unique topological phenomenon of the point-gap topology for correlated systems.

In this paper, we address the above questions by analyzing a zero-dimensional correlated system with chiral symmetry. Our analysis elucidates that correlations destroy an EP which separates two distinct topological phases in the non-interacting case; one of them is characterized by the zero-th Chern number $N_{\text{0Ch}} = 0$, and the other is characterized by $N_{\text{0Ch}} = 2$. This result indicates that the presence of correlations allows to adiabatically connect the two distinct topological phases characterized by the zero-th Chern number without closing the point-gap, which is interpreted as the reduction of the \mathbb{Z} -classification of the point-gap topology, $\mathbb{Z} \rightarrow \mathbb{Z}_2$. Furthermore, we also discover a Mott exceptional point (MEP), a unique EP for correlated systems, where only spin degrees of freedom are involved.

The rest of this paper are organized as follows. In Sec. II, we briefly review a zero-dimensional one-body Hamiltonian with chiral symmetry. In Sec. III, we introduce a non-Hermitian many-body Hamiltonian⁸¹ with correlations which preserves chiral symmetry. In Sec IV, we demonstrate that topological phase transition points accompanied by EPs disappear in the presence of correlations, which indicates the reduction of \mathbb{Z} -classification of the point-gap topology. We show that correlations induce the MEP in Sec. V which is accompanied by a short summary. The appendices are devoted to details of spectral flows of the non-Hermitian many-body Hamiltonian and a brief review of the reduction of topological classification for a zero-dimensional Hermitian system.

II. ONE-BODY HAMILTONIAN

Consider a two-orbital system in zero dimension whose non-interacting Hamiltonian is written as

$$h = \begin{pmatrix} i\alpha & \beta \\ \beta & -i\alpha \end{pmatrix}, \quad (1)$$

with real numbers α and β . The off-diagonal term describes hybridization between orbital A and B .

This model preserves chiral symmetry which satisfies

$$\tau_3 h^\dagger \tau_3 = -h, \quad (2)$$

where τ 's denote the Pauli matrices. This relation imposes the following constraint on the spectrum of h : the eigenvalues ϵ_+ and ϵ_- are pure-imaginary or form a pair, $\epsilon_- = -\epsilon_+^*$. Namely, the symmetry requires the spectrum to be symmetric about the imaginary axis. In Figs. 1(a) and 1(b), eigenvalues are plotted where we can see that the eigenvalues satisfy the above constraint.

We note that for $\alpha \neq \beta$, the point-gap at $\epsilon_{\text{ref}} = 0$ opens; no eigenvalue is equal to $\epsilon_{\text{ref}} = 0$, where ϵ_{ref} denotes the reference energy. In this case, the point-gap topology is characterized by the zero-th Chern number which is the number of eigenstates with the negative eigenvalue of

$$-i\tau_3 h = \alpha\tau_0 + \beta\tau_2. \quad (3)$$

Here, τ_0 is the identity matrix. We note that $N_{0\text{Ch}}$ takes an arbitrary integer in the generic case, while it takes 0, 1, or 2 for this model. The phase diagram is plotted in Fig. 1(c). For $(\alpha, \beta) = (0.5, 0)$, the zero-th Chern number takes $N_{0\text{Ch}} = 0$. Increasing β , the zero-th Chern number jumps from $N_{0\text{Ch}} = 0$ to 1 for $\beta = \alpha = 0.5$ [see the red line illustrated in Fig. 1(c)]. Correspondingly, the point-gap at $\epsilon_{\text{ref}} = 0$ closes on this topological transition point due to the emergence of an EP.

In the above, we have seen the EP on the topological transition point which separates the two phases of h characterized by $N_{0\text{Ch}}$; one of them is characterized by $N_{0\text{Ch}} = 0$ and the other is characterized by $N_{0\text{Ch}} = 1$ [see Fig. 1(c)]. This fact indicates the \mathbb{Z} -classification of the point-gap topology with chiral symmetry.

III. MANY-BODY HAMILTONIAN

A. Correlated model

Now, let us consider the following model with correlations

$$\hat{H} = \hat{H}_0 + \hat{H}_\mu + \hat{H}_U, \quad (4a)$$

$$\hat{H}_0 = \hat{\Psi}^\dagger \begin{pmatrix} h & 0 \\ 0 & rh \end{pmatrix} \hat{\Psi}, \quad (4b)$$

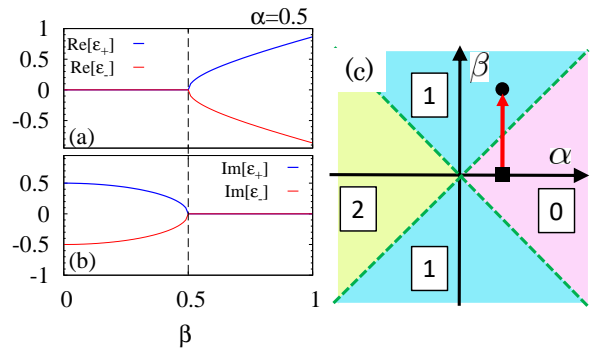


FIG. 1. (a) [(b)]: The real and imaginary parts of ϵ_+ and ϵ_- as functions of β for $\alpha = 0.5$. (c): Phase diagram of the one-body Hamiltonian h . The Hamiltonian h is characterized by the zero-th Chern number which is denoted by numbers in squares. For $\alpha = \beta$ and $\alpha = -\beta$, the zero-th Chern number jumps. The black square (dot) in this panel denotes the point $(\alpha, \beta) = (0.5, 0)$ [(0.5, 1)]. With increasing β along with the red arrow, the system shows an EP at $\alpha = \beta = 0.5$ [see panels (a) and (b)].

$$\hat{\Psi} = (\hat{c}_{A\uparrow}, \hat{c}_{B\uparrow}, \hat{c}_{A\downarrow}, \hat{c}_{B\downarrow})^T, \quad (4c)$$

$$\hat{H}_\mu = i\mu(\hat{N}_\uparrow - 1) + ir\mu(\hat{N}_\downarrow - 1), \quad (4d)$$

$$\hat{H}_U = U \sum_{l=A,B} \left(\hat{n}_{l\uparrow} - \frac{1}{2} \right) \left(\hat{n}_{l\downarrow} - \frac{1}{2} \right). \quad (4e)$$

Here, \hat{c}_{ls}^\dagger (\hat{c}_{ls}) creates (annihilates) a fermion in orbital $l = A, B$ and spin state $s = \uparrow, \downarrow$. The number operator of up-spin states (down-spin states) is defined as $\hat{N}_\uparrow = \sum_l \hat{n}_{l\uparrow}$ ($\hat{N}_\downarrow = \sum_l \hat{n}_{l\downarrow}$) with $\hat{n}_{ls} = \hat{c}_{ls}^\dagger \hat{c}_{ls}$. Interaction strength is described by a real number $U \geq 0$, and μ is a real number. The factor r ($0 < r \leq 1$) is introduced for a technical reason⁸². We consider that the above Hamiltonian is relevant to open quantum systems with one-body loss under continuous observations.

For $U = 0$, the Hamiltonian is decomposed to

$$\hat{H}_0 + \hat{H}_\mu = \hat{H}_{0\uparrow} + \hat{H}_{0\downarrow}. \quad (5)$$

Here, $\hat{H}_{0\uparrow}$ ($\hat{H}_{0\downarrow}$) acts only on fermions in up-spin states (down-spin states).

B. Symmetry of the many-body Hamiltonian

The Hamiltonian is chiral symmetric

$$\hat{\Xi} \hat{H} \hat{\Xi}^{-1} = \hat{H}, \quad (6a)$$

$$\hat{\Xi} = \prod_s (\hat{c}_{As}^\dagger + \hat{c}_{As})(\hat{c}_{Bs}^\dagger - \hat{c}_{Bs}), \quad (6b)$$

with operator \mathcal{K} taking complex conjugate. Here, $\hat{\Xi}$ is written as a product of a time-reversal operator and a particle-hole operator.

For $\mu = U = 0$, the chiral symmetry of the many-body Hamiltonian is reduced to Eq. (2), which can be confirmed as follows^{83,84}. Noting the relation

$$\hat{\Xi}\hat{\Psi}\hat{\Xi}^{-1} = \begin{pmatrix} \tau_3 & \\ & \tau_3 \end{pmatrix} \hat{\Psi}^*, \quad (7)$$

with

$$\hat{\Psi}^* = (\hat{c}_{A\uparrow}^\dagger, \hat{c}_{B\uparrow}^\dagger, \hat{c}_{A\downarrow}^\dagger, \hat{c}_{B\downarrow}^\dagger)^T, \quad (8)$$

we obtain

$$\begin{aligned} \hat{\Xi}\hat{H}_0\hat{\Xi}^{-1} &= \hat{\Psi}^T \begin{pmatrix} \tau_3 h^* \tau_3 & 0 \\ 0 & \tau_3 r h^* \tau_3 \end{pmatrix} \hat{\Psi}^*, \\ &= \hat{\Psi}^\dagger \begin{pmatrix} -\tau_3 h^\dagger \tau_3 & 0 \\ 0 & -\tau_3 r h^\dagger \tau_3 \end{pmatrix} \hat{\Psi}. \end{aligned} \quad (9)$$

Here, from the first to the second line, we have used the fact that h is a traceless matrix. The minus sign in the second line arises from the fermionic statistics. Thus, for $U = 0$, Eq. (6) is reduced to Eq. (2), indicating that \hat{H}_0 satisfies $\hat{\Xi}\hat{H}_0\hat{\Xi}^{-1} = \hat{H}_0$ when h is chiral symmetric.

We note that \hat{H}_μ and \hat{H}_U are also chiral symmetric which can be seen by noting the relation

$$\hat{\Xi}\hat{n}_{ls}\hat{\Xi}^{-1} = 1 - \hat{n}_{ls}. \quad (10)$$

Thus, the many-body Hamiltonian is chiral symmetric for arbitrary values of μ and U [see Eq. (6)].

The eigenvalues E_n ($n = 1, 2, \dots$) of the many-body Hamiltonian satisfying Eq. (6) are real or form pairs satisfying

$$E_{n'} = E_n^*. \quad (11)$$

Here, we note a crucial difference between symmetry constraints Eqs. (2) and (6). As seen in Sec. II, the constraint on the one-body Hamiltonian [Eq. (2)] requires the spectrum of h to be symmetric about the imaginary axis. In contrast, the constraint on the many-body Hamiltonian requires the spectrum of \hat{H} to be symmetric about the real axis [see Eq. (11)]. The difference arises from the fact that the chiral symmetry of the many-body Hamiltonian [Eq. (6)] is mathematically the same as the time-reversal symmetry; we note that the operator of the particle-hole transformation is unitary in the second quantized form.

We also note that the Hamiltonian \hat{H} commutes with $\hat{N}_{\text{tot}} = \sum_{ls} \hat{n}_{ls}$ and $\hat{S}_{\text{tot}}^z = (\hat{N}_\uparrow - \hat{N}_\downarrow)/2$.

IV. REDUCTION OF TOPOLOGICAL CLASSIFICATION OF POINT-GAP TOPOLOGY

We show that the EP discussed in Sec. II vanishes due to the correlation effects. This fact indicates that correlations allow to continuously connect two distinct topological phases of free fermions with maintaining the point-gap at $E_{\text{ref}} = 0$; the one of them is characterized by $N_{\text{Ch}} = 0$, and the other is characterized by $N_{\text{Ch}} = 2$.

A. Case for $U = 0$

Let us start with the spectrum for $U = 0$ which can be obtained from eigenvalues of h . We recall that the Hamiltonian can be block-diagonalized with operators \hat{N}_{tot} and \hat{S}_{tot}^z .

Figures 2(a) and 2(b) plot the spectrum as a function of β for $\alpha = 0.5$. Here, we set μ to 3 ($\mu = 3$) in order to focus on the topology of subsector with $(\hat{N}_{\text{tot}}, 2\hat{S}_{\text{tot}}^z) = (2, 0)$. In these figures, we can see that the system closes the

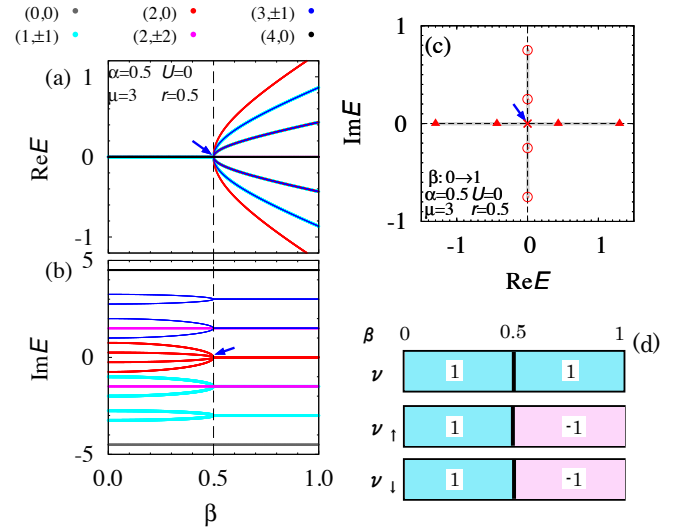


FIG. 2. (a) [(b)]: The real and imaginary parts of eigenvalues as functions of β . Colors denote eigenvalues for subsectors with $(\hat{N}_{\text{tot}}, 2\hat{S}_{\text{tot}}^z)$. (c): Spectral flow for subsector with $(\hat{N}_{\text{tot}}, 2\hat{S}_{\text{tot}}^z) = (2, 0)$. Circles, crosses, and triangles denote eigenvalues for $\beta = 0, 0.5$, and 1 , respectively. With increasing β from 0 to 1 , eigenvalues flow along gray lines. (d): \mathbb{Z}_2 -invariants as functions of β . At $\alpha = \beta = 0.5$, the point-gap at $E_{\text{ref}} = 0$ closes. These data are obtained for $\alpha = 0.5$, $U = 0$, $\mu = 3$, and $r = 0.5$

point-gap at $E_{\text{ref}} = 0$ by showing an EP at zero-energy [see blue arrows]. Here, $E_{\text{ref}} = 0$ denotes the reference energy. This EP is also observed in Fig. 2(c) where a spectral flow⁸⁵ for subsector with $(\hat{N}_{\text{tot}}, 2\hat{S}_{\text{tot}}^z) = (2, 0)$ is plotted. At $\beta = 0$, energy eigenvalues are pure-imaginary as denoted by open circles. Increasing β , we can see that the EP emerges at $\beta = 0.5$ as denoted by the cross. At $\beta = 1$, energy eigenvalues are real as denoted by triangles.

This EP of the many-body Hamiltonian \hat{H} is induced by the topological transition of the one-body Hamiltonian h . Namely, as discussed in Sec. II, the zero-th Chern number N_{Ch} jumps from 0 to 1 for $\alpha = \beta = 0.5$. Correspondingly, the point-gap of h at $\epsilon_{\text{ref}} = 0$ closes, which inducing the EP [see Figs. 1(a) and 1(b)]. We also note that \hat{H}_μ is zero for subsector with $(\hat{N}_{\text{tot}}, 2\hat{S}_{\text{tot}}^z) = (2, 0)$.

For the other sectors, the system shows EPs at $E = \pm 3i$ and $\pm 1.5i$ [see Figs. 2(a) and 2(b)], which can also be understood in terms of h because \hat{H}_μ is reduced to a constant value for each sector⁸⁶ specified by \hat{N}_{tot} and

\hat{S}_{tot}^z . As seen in Appendix A, the spectrum is symmetric about the real axis for $0 \leq \beta \leq 1$ due to the chiral symmetry [Eq. (6)].

In the above, we have seen the emergence of the EP at $E = 0$ which separates two distinct topological phases; one of them is characterized by $N_{\text{0Ch}} = 0$, and the other is characterized by $N_{\text{0Ch}} = 2$. Here, we have taken into account spin degrees of freedom.

B. Case for $U > 0$

We show that the EP at $E = 0$ is fragile against the interaction. This fragility of the EP implies the reduction of topological classification of the point-gap topology $\mathbb{Z} \rightarrow \mathbb{Z}_2$; correlations allow to continuously connect the topological phase characterized by $N_{\text{0Ch}} = 0$ and the one characterized by $N_{\text{0Ch}} = 2$ without closing the point-gap at $E_{\text{ref}} = 0$.

As a first step to understand the fragility of the EP at $E = 0$, we recall that the symmetry constraint of the many-body Hamiltonian is mathematically equivalent to that of the time-reversal symmetry [see Eq. (6)], which differs from the constraint on the one-particle Hamiltonian h [see Eq. (2)]. This fact indicates that the point-gap topology of the many-body Hamiltonian is characterized by the following \mathbb{Z}_2 -invariant²

$$\nu = \text{sgn}[\det(\hat{H} - E_{\text{ref}})], \quad (12)$$

with the reference energy $E_{\text{ref}} \in \mathbb{R}$. In the non-interacting case, we can see that the two pairs of energy eigenvalues touch at $E = 0$ for $\alpha = \beta$ with increasing β [see Figs. 2(a)-2(c)]. Correspondingly, for $E_{\text{ref}} = 0$, topological invariants ν_{\uparrow} and ν_{\downarrow} jump from 1 to -1 [see Fig. 2(d)], where ν_{\uparrow} (ν_{\downarrow}) is defined by replacing \hat{H} to $\hat{H}_{0\uparrow}$ ($\hat{H}_{0\downarrow}$) in Eq. (12)⁸⁷. Computing the \mathbb{Z}_2 -invariant ν for $U = 0$, we can see that ν does not change its value for $0 \leq \beta \leq 1$ [see Fig. 2(d)], although the EP at $E = 0$ is observed for $\alpha = \beta = 0.5$ [see Fig. 2]. Noting that for $U > 0$, ν is the only topological invariant⁸⁸ among ν , ν_{\uparrow} , and ν_{\downarrow} , we can conclude that the EP at $E = 0$ is fragile against correlations.

The fragility of the EP at $E = 0$ is also observed by computing spectrum of the many-body Hamiltonian. Figures 3(a)-3(c) elucidate the absence of the EPs at $E = 0$ which are observed in the non-interacting case⁸⁹; although we observe an EP for $U = 1$, it emerges away from $E = 0$. These results are consistent with the \mathbb{Z}_2 -invariant ν ; the point-gap at $E_{\text{ref}} = 0$ remains open for $\alpha = 0.5$ and $0 \leq \beta \leq 1$, corresponding to the fact that ν does not change its value.

In addition, Fig. 3(d) indicates that the point-gap at $E_{\text{ref}} = 0$ also remains open under the following deformation: increasing U from 0 to 1 for $(\alpha, \beta) = (0.5, 0)$; decreasing U from 1 to 0 for $(\alpha, \beta) = (0.5, 1)$.

The above results [see Figs. 3(c) and 3(d)] indicate that correlation effects allow to connect two topological phases

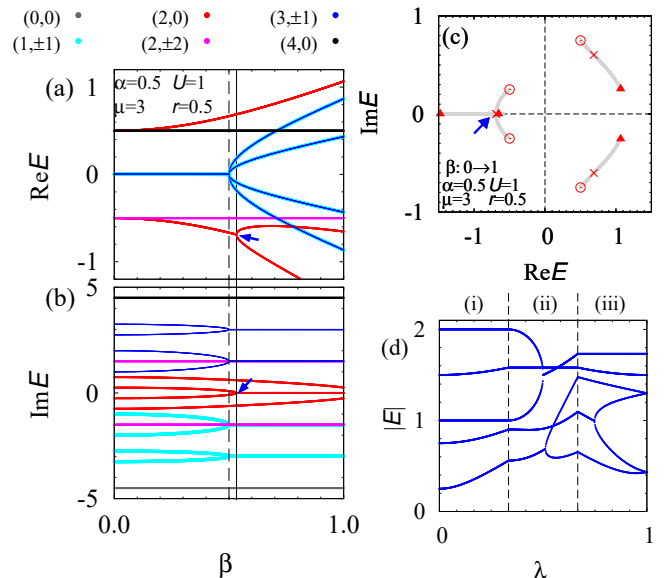


FIG. 3. (a) [(b)]: The real and imaginary parts of eigenvalues as functions of β . Colors denote eigenvalues for subsectors with $(\hat{N}_{\text{tot}}, 2\hat{S}_{\text{tot}}^z)$. (c): Spectrum for subsector with $(\hat{N}_{\text{tot}}, 2\hat{S}_{\text{tot}}^z) = (2, 0)$. Circles, crosses, and triangles denote eigenvalues for $\beta = 0, 0.533$, and 1 , respectively. With increasing β from 0 to 1 , eigenvalues flow along gray lines. The spectral flow including other sectors is shown in Appendix A. In panels (a), (b), and (c), blue arrows denote an EP away from $E = 0$ which cannot be described by the one-body Hamiltonian h . (d): The absolute value of eigenvalues as functions of λ . The reference energy is $|E_{\text{ref}}| = 0$. Here, λ parameterizes a deformation as follows: (i) for $0 \leq \lambda < 1/3$, it parameterizes as $(U, \beta) = (3\lambda, 0)$; (ii) for $1/3 \leq \lambda < 2/3$, it parameterizes as $(U, \beta) = (1, 3\lambda - 1)$; (iii) for $2/3 \leq \lambda < 1$, it parameterizes as $(U, \beta) = (3 - 3\lambda, 1)$. In panel (d), dashed vertical lines denote $\lambda = 1/3$ and $\lambda = 2/3$, respectively. These data are obtained for $\alpha = 0.5$, $\mu = 3$, and $r = 0.5$.

for $(\alpha, \beta) = (0.5, 0)$ and $(0.5, 1)$ without closing the point-gap at $E_{\text{ref}} = 0$. The former (latter) is characterized by $N_{\text{0Ch}} = 0$ ($N_{\text{0Ch}} = 2$) in the non-interacting case. This behavior is reminiscent of the reduction of topological classification; for instance, in a zero-dimensional topological system, the topology of the one-body Hamiltonian is characterized by a \mathbb{Z} -invariant while the topology of two copies of them are fragile against the interactions (for more details of the Hermitian case, see Appendix B). We would like to stress that the interaction is essential for this phenomenon as is the case of a Hermitian system⁷⁵. Namely, without any interaction term, one cannot avoid the topological transition.

V. MOTT EXCEPTIONAL POINT

In the above, we have seen that the point-gap at $E_{\text{ref}} = 0$ remains open while the EP emerges away from $E = 0$. In this section, we show that this EP corresponds to the

MEP, a unique EP for correlated systems, where only spin degrees of freedom are involved.

Firstly, we recall that for the non-interacting case, the EPs are fixed to the imaginary axis [see Figs. 2(a), 2(b), and 5] because the eigenvalues are governed by the one-body Hamiltonian h . In contrast to these EPs for $U = 0$, the MEP emerges away from the imaginary axis [see Fig. 6(c)], which indicates that interactions are essential.

For better understanding of this MEP, we apply the second order perturbation theory by supposing that the interaction U is sufficiently large $U \gg \alpha, \beta$. In such a case, an EP emerges around $\text{Re}E = -U/2$. At $\alpha = \beta = 0$, this band touching is described by the following two states:

$$|\Psi_1\rangle = \hat{c}_{A\uparrow}^\dagger \hat{c}_{B\downarrow}^\dagger |0\rangle, \quad (13)$$

$$|\Psi_2\rangle = \hat{c}_{A\downarrow}^\dagger \hat{c}_{B\uparrow}^\dagger |0\rangle. \quad (14)$$

For this subspace, we can obtain the effective Hamiltonian

$$\begin{aligned} \hat{H}_{\text{eff}} = & -\frac{U}{2} + i\alpha(1-r) \sum_l \text{sgn}(l) \hat{S}_l^z + \frac{(1+r^2)}{2} J \hat{S}_A^z \hat{S}_B^z \\ & + rJ(\hat{S}_A^x \hat{S}_B^x + \hat{S}_A^y \hat{S}_B^y) - \frac{J(1+r^2)}{8}, \end{aligned} \quad (15)$$

with $J = 4\beta^2/U$. Here, \hat{S}_l^μ ($\mu = x, y, z$) are spin operators; $\hat{S}_l^z = (\hat{n}_{l\uparrow} - \hat{n}_{l\downarrow})/2$, $\hat{S}_l^x = (\hat{S}_l^+ + \hat{S}_l^-)/2$, and $\hat{S}_l^y = (\hat{S}_l^+ - \hat{S}_l^-)/(2i)$ with $\hat{S}_l^+ = \hat{c}_{l\uparrow}^\dagger \hat{c}_{l\downarrow}$ and $\hat{S}_l^- = \hat{c}_{l\downarrow}^\dagger \hat{c}_{l\uparrow}$. In a matrix form, the effective Hamiltonian and the operator $\hat{\Xi}$ are rewritten as

$$\hat{H}_{\text{eff}} = E_0 \rho_0 + \frac{rJ}{2} \rho_1 + i\alpha(1-r) \rho_3, \quad (16a)$$

$$\hat{\Xi} = \rho_1 \mathcal{K}, \quad (16b)$$

with $E_0 = -U/2 - J(1+r^2)/4$. Here, ρ_0 and ρ 's are the identity matrix and the Pauli matrices, respectively. Diagonalizing the Hamiltonian, we have

$$E = E_0 \pm \sqrt{\left(\frac{rJ}{2}\right)^2 - \alpha^2(1-r)^2}. \quad (17)$$

Thus, for $J = J_c := 2\alpha(1-r)/r$, we have an EP. Here, we would like to stress that the above EP is described by the effective spin model (16), which indicates that correlations are essential for the MEP.

Because H_{eff} preserves the chiral symmetry, we can characterize the MEP by the \mathbb{Z}_2 -invariant

$$\nu_{\text{eff}} = \text{sgn}[\det(H_{\text{eff}} - E_0 \rho_0)]. \quad (18)$$

Here, we have fixed the reference energy to $E_{\text{ref}} = E_0$. By substituting Eq. (16a) to Eq. (18), we obtain ν_{eff} taking 1 (-1) for $J < J_c$ ($J > J_c$). This result is consistent with the \mathbb{Z}_2 -invariant computed from the original Hamiltonian \hat{H} . Figure 4 shows that the \mathbb{Z}_2 -invariant jumps at $\beta_c \sim$

0.53, which indicates that the invariant jumps at $J \sim 1.12$.

We note that the difference of the MEP from the ordinary EP for $U = 0$ can also be seen by turning off μ (see Appendix C).

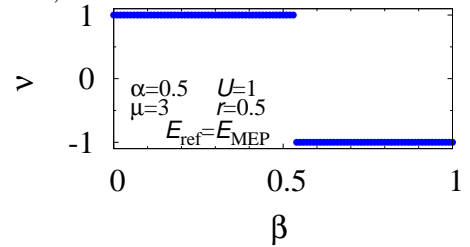


FIG. 4. The \mathbb{Z}_2 -invariant as a function of β . Here, the reference energy is set to $E_{\text{ref}} = E_{\text{MEP}} = -0.6886$ where the MEP emerges. The data are obtained for $\alpha = 0.5$, $U = 1$, $\mu = 3$, and $r = 0.5$.

VI. SUMMARY AND DISCUSSION

In this paper, we have analyzed correlation effects on the point-gap topology in the zero-dimensional system with chiral symmetry. Our analysis elucidates that correlations destroy the EP which separates two distinct topological phases characterized by the zero-th Chern number; one of them is characterized by $N_{0\text{Ch}} = 0$ and the other is characterized by $N_{0\text{Ch}} = 2$. This result originates from the fact that the many-body chiral symmetry results in the \mathbb{Z}_2 -invariant, in contrast to the \mathbb{Z} -invariant in the non-interacting case. The above results suggest that correlations change \mathbb{Z} -classification of free fermions to \mathbb{Z}_2 -classification, which is reminiscent of the reduction of topological classification in Hermitian systems. Furthermore, we have discovered the MEP for which correlations are essential. The MEP is described by the effective spin Hamiltonian (i.e., charge degrees of freedom are not involved).

We finish this paper with a remark on the case of higher dimensions. Because Eqs. (2) and (6) should hold also for higher dimensions, the topological properties of the many-body Hamiltonian may differ from those of the one-body Hamiltonian for even spatial dimensions.

ACKNOWLEDGMENTS

T.Y. thanks Yoshihito Kuno for fruitful discussion. This work is supported by JPSP Grant-in-Aid for Scientific Research on Innovative Areas “Discrete Geometric Analysis for Materials Design”: Grants No. JP20H04627 (T.Y.). This work is also supported by the JSPS KAKENHI, Grants No JP17H06138 and No. JP21K13850.

- ¹ H. Shen, B. Zhen, and L. Fu, *Phys. Rev. Lett.* **120**, 146402 (2018).
- ² Z. Gong, Y. Ashida, K. Kawabata, K. Takasan, S. Higashikawa, and M. Ueda, *Phys. Rev. X* **8**, 031079 (2018).
- ³ K. Kawabata, S. Higashikawa, Z. Gong, Y. Ashida, and M. Ueda, *Nature Communications* **10**, 297 (2019).
- ⁴ K. Kawabata, K. Shiozaki, M. Ueda, and M. Sato, *Phys. Rev. X* **9**, 041015 (2019).
- ⁵ H. Zhou and J. Y. Lee, *Phys. Rev. B* **99**, 235112 (2019).
- ⁶ E. J. Bergholtz, J. C. Budich, and F. K. Kunst, *Rev. Mod. Phys.* **93**, 015005 (2021).
- ⁷ T. Yoshida, R. Peters, N. Kawakami, and Y. Hatsugai, *Progress of Theoretical and Experimental Physics* **2020**, 12A109 (2020).
- ⁸ Y. Ashida, Z. Gong, and M. Ueda, *Advances in Physics* **69**, 249 (2020).
- ⁹ N. Hatano and D. R. Nelson, *Phys. Rev. Lett.* **77**, 570 (1996).
- ¹⁰ C. M. Bender and S. Boettcher, *Phys. Rev. Lett.* **80**, 5243 (1998).
- ¹¹ T. Fukui and N. Kawakami, *Physical Review B* **58**, 16051 (1998).
- ¹² Y. C. Hu and T. L. Hughes, *Phys. Rev. B* **84**, 153101 (2011).
- ¹³ K. Esaki, M. Sato, K. Hasebe, and M. Kohmoto, *Phys. Rev. B* **84**, 205128 (2011).
- ¹⁴ V. M. Martinez Alvarez, J. E. Barrios Vargas, and L. E. F. Foa Torres, *Phys. Rev. B* **97**, 121401 (2018).
- ¹⁵ S. Yao and Z. Wang, *Phys. Rev. Lett.* **121**, 086803 (2018).
- ¹⁶ S. Yao, F. Song, and Z. Wang, *Phys. Rev. Lett.* **121**, 136802 (2018).
- ¹⁷ F. K. Kunst, E. Edvardsson, J. C. Budich, and E. J. Bergholtz, *Phys. Rev. Lett.* **121**, 026808 (2018).
- ¹⁸ C. H. Lee and R. Thomale, *Phys. Rev. B* **99**, 201103 (2019).
- ¹⁹ E. Edvardsson, F. K. Kunst, and E. J. Bergholtz, *Phys. Rev. B* **99**, 081302 (2019).
- ²⁰ D. S. Borgnia, A. J. Kruchkov, and R.-J. Slager, *Phys. Rev. Lett.* **124**, 056802 (2020).
- ²¹ K. Yokomizo and S. Murakami, *Phys. Rev. Lett.* **123**, 066404 (2019).
- ²² J. C. Budich, J. Carlström, F. K. Kunst, and E. J. Bergholtz, *Phys. Rev. B* **99**, 041406 (2019).
- ²³ T. Yoshida, R. Peters, N. Kawakami, and Y. Hatsugai, *Phys. Rev. B* **99**, 121101 (2019).
- ²⁴ R. Okugawa and T. Yokoyama, *Phys. Rev. B* **99**, 041202 (2019).
- ²⁵ H. Zhou, J. Y. Lee, S. Liu, and B. Zhen, *Optica* **6**, 190 (2019).
- ²⁶ K. Kimura, T. Yoshida, and N. Kawakami, *Phys. Rev. B* **100**, 115124 (2019).
- ²⁷ K. Kawabata, T. Bessho, and M. Sato, *Phys. Rev. Lett.* **123**, 066405 (2019).
- ²⁸ Z. Yang, A. P. Schnyder, J. Hu, and C.-K. Chiu, *Phys. Rev. Lett.* **126**, 086401 (2021).
- ²⁹ P. Delplace, T. Yoshida, and Y. Hatsugai, *arXiv preprint arXiv:2103.08232* (2021).
- ³⁰ K. Zhang, Z. Yang, and C. Fang, *Phys. Rev. Lett.* **125**, 126402 (2020).
- ³¹ N. Okuma, K. Kawabata, K. Shiozaki, and M. Sato, *Phys. Rev. Lett.* **124**, 086801 (2020).
- ³² T. Hofmann, T. Helbig, F. Schindler, N. Salgo, M. Brzezińska, M. Greiter, T. Kiessling, D. Wolf, A. Vollhardt, A. Kabaši, C. H. Lee, A. Bilušić, R. Thomale, and T. Neupert, *Phys. Rev. Research* **2**, 023265 (2020).
- ³³ L. Xiao, T. Deng, K. Wang, G. Zhu, Z. Wang, W. Yi, and P. Xue, *Nature Physics* **16**, 761 (2020).
- ³⁴ T. Yoshida, T. Mizoguchi, and Y. Hatsugai, *Phys. Rev. Research* **2**, 022062 (2020).
- ³⁵ R. Okugawa, R. Takahashi, and K. Yokomizo, *Phys. Rev. B* **102**, 241202 (2020).
- ³⁶ K. Kawabata, M. Sato, and K. Shiozaki, *Phys. Rev. B* **102**, 205118 (2020).
- ³⁷ Y. Fu and S. Wan, *arXiv preprint arXiv:2008.09033* (2020).
- ³⁸ K. Kawabata, K. Shiozaki, and S. Ryu, *arXiv preprint arXiv:2011.11449* (2020).
- ³⁹ T. E. Lee, *Phys. Rev. Lett.* **116**, 133903 (2016).
- ⁴⁰ Y. Xu, S.-T. Wang, and L.-M. Duan, *Phys. Rev. Lett.* **118**, 045701 (2017).
- ⁴¹ S. Diehl, E. Rico, M. A. Baranov, and P. Zoller, *Nature Physics* **7**, 971 (2011).
- ⁴² C.-E. Bardyn, M. A. Baranov, C. V. Kraus, E. Rico, A. İmamoglu, P. Zoller, and S. Diehl, *New Journal of Physics* **15**, 085001 (2013).
- ⁴³ S. Lieu, M. McGinley, and N. R. Cooper, *Phys. Rev. Lett.* **124**, 040401 (2020).
- ⁴⁴ A. Guo, G. J. Salamo, D. Duchesne, R. Morandotti, M. Volatier-Ravat, V. Aimez, G. A. Siviloglou, and D. N. Christodoulides, *Phys. Rev. Lett.* **103**, 093902 (2009).
- ⁴⁵ C. E. Rüter, K. G. Makris, R. El-Ganainy, D. N. Christodoulides, M. Segev, and D. Kip, *Nature physics* **6**, 192 (2010).
- ⁴⁶ A. Regensburger, C. Bersch, M.-A. Miri, G. Onishchukov, D. N. Christodoulides, and U. Peschel, *Nature* **488**, 167 (2012).
- ⁴⁷ B. Zhen, C. W. Hsu, Y. Igarashi, L. Lu, I. Kaminer, A. Pick, S.-L. Chua, J. D. Joannopoulos, and M. Soljačić, *Nature* **525**, 354 EP (2015).
- ⁴⁸ A. U. Hassan, B. Zhen, M. Soljačić, M. Khajavikhan, and D. N. Christodoulides, *Phys. Rev. Lett.* **118**, 093002 (2017).
- ⁴⁹ K. Takata and M. Notomi, *Phys. Rev. Lett.* **121**, 213902 (2018).
- ⁵⁰ H. Zhou, C. Peng, Y. Yoon, C. W. Hsu, K. A. Nelson, L. Fu, J. D. Joannopoulos, M. Soljačić, and B. Zhen, *Phys. Rev. Lett.* **359**, 1009 (2018).
- ⁵¹ H. Zhou, C. Peng, Y. Yoon, C. W. Hsu, K. A. Nelson, L. Fu, J. D. Joannopoulos, M. Soljačić, and B. Zhen, *Phys. Rev. Lett.* **359**, 1009 (2018).
- ⁵² T. Ozawa, H. M. Price, A. Amo, N. Goldman, M. Hafezi, L. Lu, M. C. Rechtsman, D. Schuster, J. Simon, O. Zilberberg, and I. Carusotto, *Rev. Mod. Phys.* **91**, 015006 (2019).
- ⁵³ T. Yoshida and Y. Hatsugai, *Phys. Rev. B* **100**, 054109 (2019).
- ⁵⁴ A. Ghatak, M. Brandenbourger, J. van Wezel, and C. Coulais, *Phys. Rev. Lett.* **117**, 29561 (2020).
- ⁵⁵ C. Scheibner, W. T. M. Irvine, and V. Vitelli, *Phys. Rev. Lett.* **125**, 118001 (2020).
- ⁵⁶ V. Kozii and L. Fu, *arXiv preprint arXiv:1708.05841* (2017).

- ⁵⁷ A. A. Zyuzin and A. Y. Zyuzin, Phys. Rev. B **97**, 041203 (2018).
- ⁵⁸ T. Yoshida, R. Peters, and N. Kawakami, Phys. Rev. B **98**, 035141 (2018).
- ⁵⁹ H. Shen and L. Fu, Phys. Rev. Lett. **121**, 026403 (2018).
- ⁶⁰ M. Papaj, H. Isobe, and L. Fu, Phys. Rev. B **99**, 201107 (2019).
- ⁶¹ T. Matsushita, Y. Nagai, and S. Fujimoto, Phys. Rev. B **100**, 245205 (2019).
- ⁶² T. Matsushita, Y. Nagai, and S. Fujimoto, arXiv preprint arXiv:2004.11014 (2020).
- ⁶³ T. Yoshida, K. Kudo, and Y. Hatsugai, Scientific Reports **9**, 16895 (2019).
- ⁶⁴ N. Matsumoto, K. Kawabata, Y. Ashida, S. Furukawa, and M. Ueda, Phys. Rev. Lett. **125**, 260601 (2020).
- ⁶⁵ C.-X. Guo, X.-R. Wang, and S.-P. Kou, EPL (Europhysics Letters) **131**, 27002 (2020).
- ⁶⁶ T. Yoshida, K. Kudo, H. Katsura, and Y. Hatsugai, Phys. Rev. Research **2**, 033428 (2020).
- ⁶⁷ Q. Zhang, W.-T. Xu, Z.-Q. Wang, and G.-M. Zhang, Communications Physics **3**, 209 (2020).
- ⁶⁸ H. Shackleton and M. S. Scheurer, Phys. Rev. Research **2**, 033022 (2020).
- ⁶⁹ D.-W. Zhang, Y.-L. Chen, G.-Q. Zhang, L.-J. Lang, Z. Li, and S.-L. Zhu, Phys. Rev. B **101**, 235150 (2020).
- ⁷⁰ T. Liu, J. J. He, T. Yoshida, Z.-L. Xiang, and F. Nori, Phys. Rev. B **102**, 235151 (2020).
- ⁷¹ Z. Xu and S. Chen, Phys. Rev. B **102**, 035153 (2020).
- ⁷² L. Pan, X. Wang, X. Cui, and S. Chen, Phys. Rev. A **102**, 023306 (2020).
- ⁷³ K. Yang, S. C. Morampudi, and E. J. Bergholtz, Phys. Rev. Lett. **126**, 077201 (2021).
- ⁷⁴ W. Xi, Z.-H. Zhang, Z.-C. Gu, and W.-Q. Chen, Science Bulletin (2021).
- ⁷⁵ L. Fidkowski and A. Kitaev, Phys. Rev. B **81**, 134509 (2010).
- ⁷⁶ H. Yao and S. Ryu, Phys. Rev. B **88**, 064507 (2013).
- ⁷⁷ S. Ryu and S.-C. Zhang, Phys. Rev. B **85**, 245132 (2012).
- ⁷⁸ X.-L. Qi, New J. Phys. **15**, 065002 (2013).
- ⁷⁹ S. Mu, C. H. Lee, L. Li, and J. Gong, Phys. Rev. B **102**, 081115 (2020).
- ⁸⁰ C. H. Lee, arXiv preprint arXiv:2006.01182 (2020).
- ⁸¹ In zero dimension, systems are described by few particle problems. However, we use the word “many-body Hamiltonian” in order to distinguish it from one-body Hamiltonian.
- ⁸² For $r = 1$, we have eigenstates whose eigenvalues are zero. In order to have a gapped system for $\epsilon_{\text{ref}} = 0$, we set $r = 0.5$. We note that for $\epsilon_{\text{ref}} = 0$, the point-gap topology of rh is the same as that of h .
- ⁸³ Y. Hatsugai, Journal of the Physical Society of Japan **75**, 123601 (2006).
- ⁸⁴ V. Gurarie, Phys. Rev. B **83**, 085426 (2011).
- ⁸⁵ In Fig. 2(c), eigenvalues for subsector with $(\hat{N}_{\text{tot}}, 2\hat{S}_{\text{tot}}^z) = (2, 0)$ are plotted. The spectrum including the other sectors are plotted in Fig. 5.
- ⁸⁶ For subsector with $(\hat{N}_{\text{tot}}, 2\hat{S}_{\text{tot}}^z) = (1, 1)$ $[(1, -1)]$, an EP emerges at $E = -ir\mu$ ($i\mu$). For subsector with $(\hat{N}_{\text{tot}}, 2\hat{S}_{\text{tot}}^z) = (3, 1)$ $[(3, -1)]$, an EP emerges at $E = i\mu$ ($ir\mu$).
- ⁸⁷ We recall Eq. (5) indicating that the Hamiltonian \hat{H} is decomposed to $\hat{H}_{0\uparrow}$ and $\hat{H}_{0\downarrow}$ for $U = 0$.

- ⁸⁸ This is because up-spin and down-spin states are decoupled only for the non-interacting case. Only in the non-interacting case, the eigenvalues of \hat{H} is obtained by summing the eigenvalues of $\hat{H}_{0\uparrow}$ and $\hat{H}_{0\downarrow}$.
- ⁸⁹ These figures indicate the emergence of an EP away from $E = 0$. For this EP, correlation effects is essential (see for more details, see Sec. V).

Appendix A: Details of spectral flows

Here, we plot the spectral flow of \hat{H} in the complex plane. Figure 5 indicates the spectral flow for $U = 0$. In this case, with increasing β from 0 to 1, we can see that a topological phase transition occurs at $\beta = \alpha$ [see also Fig. 1]. Correspondingly, an EP emerges, and the point-gap at $E_{\text{ref}} = 0$ closes for $\alpha = \beta$.

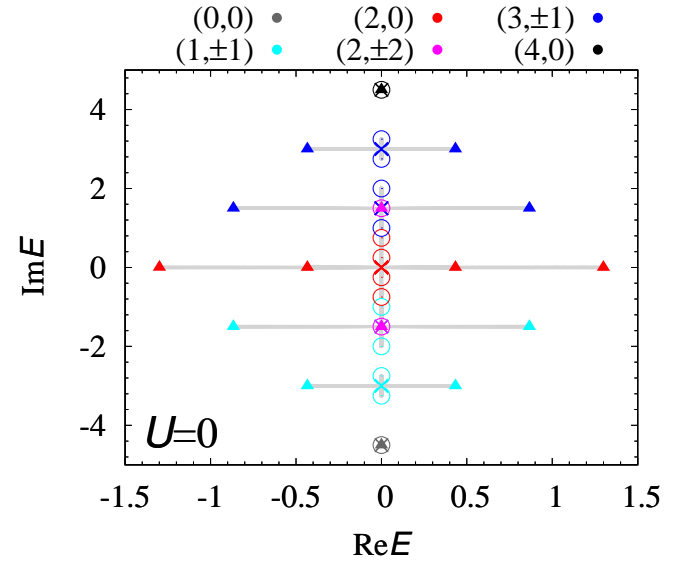


FIG. 5. Spectral flow for each subsector with $(\hat{N}_{\text{tot}}, 2\hat{S}_{\text{tot}}^z)$. Circles, crosses, and triangles denote eigenvalues for $\beta = 0, 0.5, 1$, respectively. With increasing β from 0 to 1, eigenvalues flow along gray lines. These data are obtained for $U = 0, \alpha = 0.5, \mu = 3$, and $r = 0.5$.

In contrast to the gap-closing observed for $U = 0$, the point-gap at $E_{\text{ref}} = 0$ remains open for $U = 1$. Figure 6 indicates the spectral flow for $U = 1$. This figure shows that the point-gap at $E_{\text{ref}} = 0$ remains open for $0 \leq \beta \leq 1$.

Appendix B: Reduction of topological classification for a Hermitian case

Let us briefly review reduction of topological classification for a Hermitian system in zero dimension.

Consider a zero-dimensional Hamiltonian \hat{H}_{H0} defined as

$$\hat{H}_{\text{H0}} = \hat{\Psi}^\dagger \begin{pmatrix} h_{\text{H}} & 0 \\ 0 & rh_{\text{H}} \end{pmatrix} \hat{\Psi}, \quad (\text{B1})$$

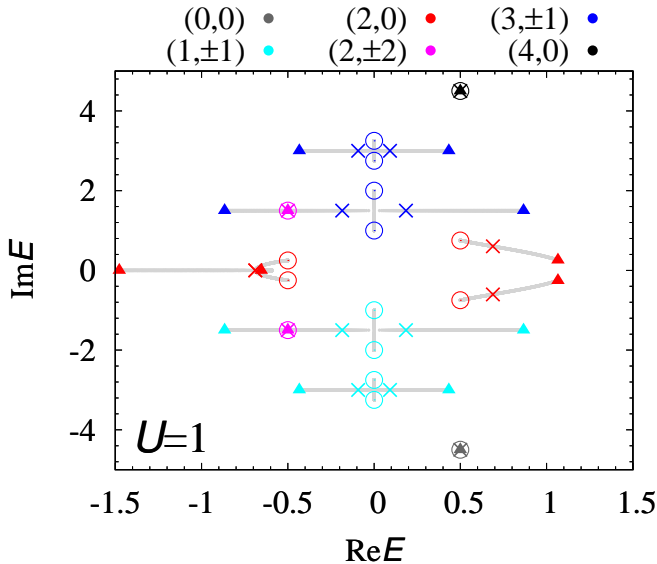


FIG. 6. Spectral flow for each subsector with $(\hat{N}_{\text{tot}}, 2\hat{S}_{\text{tot}}^z)$. Circles, crosses, and triangles denote eigenvalues for $\beta = 0, 0.533, \text{ and } 1$, respectively. With increasing β from 0 to 1, eigenvalues flow along gray lines. These data are obtained for $U = 1, \alpha = 0.5, \mu = 3$, and $r = 0.5$. We note that the eigenvalues denoted by red symbols are identical to the ones shown in Fig. 3(c).

with r ($0 \leq r \leq 1$) and $\hat{\Psi}$ defined in Eq. (4c). When the Hamiltonian is invariant under applying $\hat{U}_H = e^{i\pi\hat{T}_{\text{tot}}^z}$ with $\hat{T}_{\text{tot}}^z = \sum_s (\hat{n}_{as} - \hat{n}_{bs})/2$, the symmetry constraint $[\hat{H}_{H0}, \hat{U}_H] = 0$ is rewritten as

$$[h_H, i\tau_3] = 0, \quad (\text{B2})$$

which can be seen by noting the following relation

$$\hat{U}_H \hat{\Psi} \hat{U}_H^\dagger = \begin{pmatrix} i\tau_3 & \\ & i\tau_3 \end{pmatrix} \hat{\Psi}. \quad (\text{B3})$$

Namely, the one-body Hamiltonian h_H is written as $h_H = \alpha_0\tau_0 + \alpha\tau_3$ with real numbers α_0 and α . In the non-interacting case, the topological phase is characterized by the \mathbb{Z} -invariant, $N_{\text{ps0Ch}} = (N_{A0\text{Ch}} - N_{B0\text{Ch}})/2$, where $N_{A0\text{Ch}}$ ($N_{B0\text{Ch}}$) denotes the number of eigenstates in orbital A (B) whose eigenvalues are smaller than α_0 . Namely, for $\alpha < 0$ ($\alpha > 0$), N_{ps0Ch} of $h_H \oplus rh_H$ takes 1 (-1).

Now, we consider the following correlated model

$$\hat{H}_H = \hat{H}_{H0} + \hat{H}_{H\mu} + \hat{H}_{HV}, \quad (\text{B4a})$$

with

$$\hat{H}_{H\mu} = -\mu\hat{N}_\uparrow - r\mu\hat{N}_\downarrow, \quad (\text{B4b})$$

$$\hat{H}_{HV} = V(\hat{c}_{a\uparrow}^\dagger \hat{c}_{a\downarrow}^\dagger \hat{c}_{b\downarrow} \hat{c}_{b\uparrow} + h.c.). \quad (\text{B4c})$$

Here, μ and V are real numbers. We note that $\hat{H}_{H\mu}$ and \hat{H}_{HV} are also invariant under applying \hat{U}_H which can be confirmed by recalling Eq. (B3).

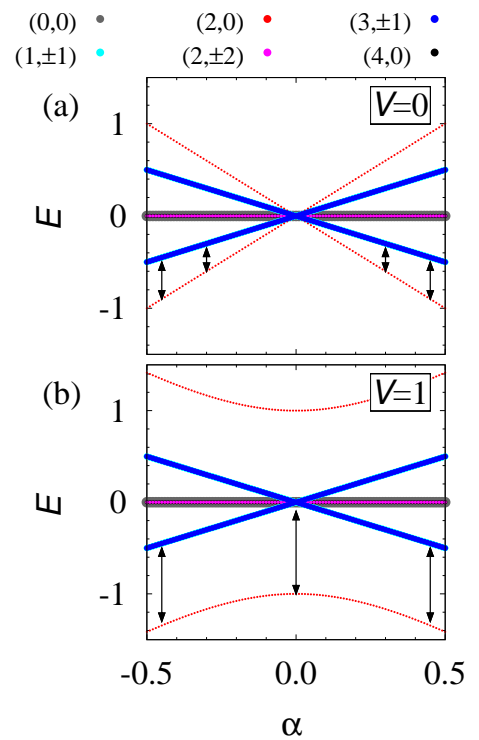


FIG. 7. (a) [(b)]: Energy spectrum of the Hamiltonian \hat{H}_H as functions of α for $V = 0$ [$V = 1$]. Colored dot denote eigenvalues for subsectors with $(\hat{N}_{\text{tot}}, 2\hat{S}_{\text{tot}}^z)$. The each eigenvalue of subsector with $(\hat{N}_{\text{tot}}, 2\hat{S}_{\text{tot}}^z) = (1, \pm 1)$ is the same as that of subsector with $(\hat{N}_{\text{tot}}, 2\hat{S}_{\text{tot}}^z) = (3, \pm 1)$. The arrows denote the gap. The data are obtained for $r = 0.5$ and $\mu = \alpha_0$.

In the presence of correlation, the topological phase characterized by $N_{\text{ps0Ch}} = 1$ can be adiabatically connected to the phase characterized by $N_{\text{ps0Ch}} = -1$. To see this, let us start with the non-interacting case. For $V = 0$, the gap closes due to the topological phase transition described by the one-body Hamiltonian h_H [see Fig. 7(a)]. In contrast to the non-interacting case, the system does not show the gap-closing for $V = 1$ [see Fig. 7(b)]. We note that each eigenstate preserves the symmetry described by \hat{U}_H .

The above results indicate that the topological phase characterized by $N_{\text{ps0Ch}} = 1$ can be adiabatically connected to the phase characterized by $N_{\text{ps0Ch}} = -1$ in the presence of the interaction. In other words, the above two phases are topologically equivalent in the presence of correlations, which implies the reduction of topological classification $\mathbb{Z} \rightarrow \mathbb{Z}_2$.

We finish this part with a remark on the non-Hermitian case. For non-Hermitian systems showing the non-trivial point-gap topology, we have defined the point-gap of the many-body Hamiltonian by introducing reference energy E_{ref} , while for the Hermitian case, the gap is defined as the energy difference between the ground state and the first excited state.

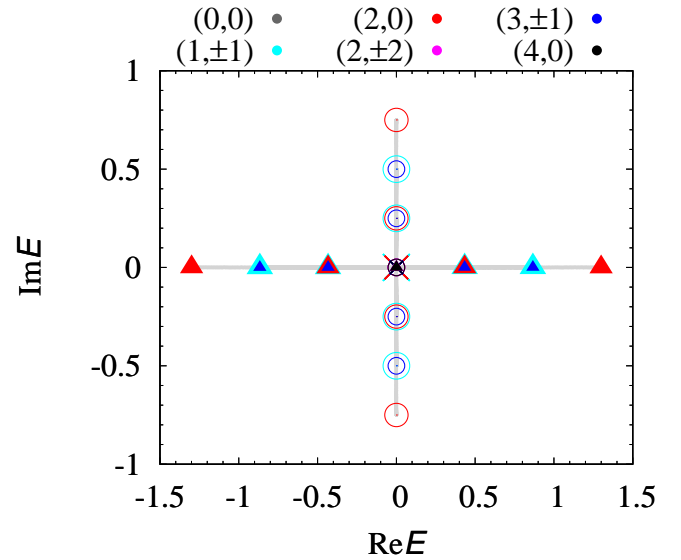
Appendix C: Details of spectral flows for $\mu = 0$


FIG. 8. Spectral flow for each subsector with $(\hat{N}_{\text{tot}}, 2\hat{S}_{\text{tot}}^z)$ at $\mu = 0$ and $U = 0$. These data are plotted in a similar way as Fig. 5. Circles, crosses, and triangles denote eigenvalues for $\beta = 0, 0.5$, and 1 , respectively. These data are obtained for $\alpha = 0.5$ and $r = 0.5$.

We discuss the spectral flow for $\mu = 0$. In Fig. 8, the spectral flow for $U = 0$ is plotted. As shown in this figure, subsectors labeled by $\hat{N}_{\text{tot}} = 1$, $\hat{N}_{\text{tot}} = 2$, and $\hat{N}_{\text{tot}} = 3$ are involved with the EP at $E = 0$, which can be understood by analyzing the one-body Hamiltonian h .

On the other hand, in the presence of the interaction, subsectors labeled by $\hat{N}_{\text{tot}} = 1$ and $\hat{N}_{\text{tot}} = 3$ are not involved with the MEP emerging away from the imaginary axis [see Fig. 9]. This fact also supports that the MEP is described by spin degrees of freedom and essentially differs from the EP in the non-interacting case.

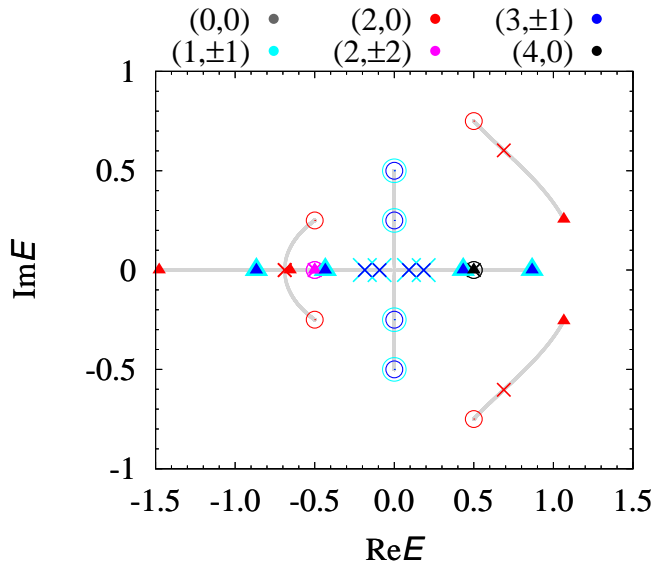


FIG. 9. Spectral flow for each subsector with $(\hat{N}_{\text{tot}}, 2\hat{S}_{\text{tot}}^z)$ at $\mu = 0$ and $U = 1$. These data are plotted in a similar way as Fig. 6. Circles, crosses, and triangles denote eigenvalues for $\beta = 0, 0.533,$ and $1,$ respectively. These data are obtained for $\alpha = 0.5$ and $r = 0.5$.